Interface currents in topological superconductor-ferromagnet heterostructures

P M R Brydon[1], Carsten Timm[2] and Andreas P Schnyder[3]

[1] Institut für Theoretische Physik, Technische Universität Dresden, D-01062 Dresden, Germany

E-mail: `brydon@theory.phy.tu-dresden.de`

[2] Institut für Theoretische Physik, Technische Universität Dresden, D-01062 Dresden, Germany

E-mail: `carsten.timm@tu-dresden.de`

[3] Max-Planck-Institut für Festkörperforschung, Heisenbergstrasse 1, D-70569 Stuttgart, Germany

E-mail: `a.schnyder@fkf.mpg.de`

Abstract. We propose the existence of a substantial charge current parallel to the interface between a noncentrosymmetric superconductor and a metallic ferromagnet. Our analysis focuses upon two complementary orbital-angular-momentum pairing states of the superconductor, exemplifying topologically nontrivial states which are gapped and gapless in the bulk, respectively. Utilizing a quasiclassical scattering theory, we derive an expression for the interface current in terms of Andreev reflection coefficients. Performing a systematic study of the current, we find stark qualitative differences between the gapped and gapless superconductors, which reflect the very different underlying topological properties. For the fully gapped superconductor, there is a sharp drop in the zero-temperature current as the system is tuned from a topologically nontrivial to a trivial phase. We explain this in terms of the sudden disappearance of the contribution to the current from the subgap edge states at the topological transition. The current in the gapless superconductor is characterized by a dramatic enhancement at low temperatures, and exhibits a singular dependence on the exchange-field strength in the ferromagnetic metal at zero temperature. This is caused by the energy shift of the strongly spin-polarized nondegenerate zero-energy flat bands due to their coupling to the exchange field. We argue that the interface current provides a novel test of the topology of the superconductor, and discuss prospects for the experimental verification of our predictions.

1. Introduction

The discovery that gapped single-particle Hamiltonians can have a nontrivial topology, depending on their dimensionality and the presence of time-reversal and particle-hole symmetries [1, 2, 3, 4, 5], has sparked a massive search for topological materials. A key motivation is to realize exotic Majorana-fermion states, which are guaranteed to appear at the edges of a fully gapped topological insulator or superconductor by the bulk-boundary correspondence [4, 5], and which may have applications in quantum computation. Parallel to these developments, the concept of topological nontriviality has been generalized to *gapless* systems, such as nodal superconductors [6, 7, 8, 9, 10, 11, 12, 13] or Weyl semimetals [14, 15]. Bulk-boundary correspondences can also be developed in these cases, leading to the topologically protected appearance of nondegenerate zero-energy (or Majorana) arc lines or flat bands at certain surfaces. Much work has now been done on understanding the conditions under which these states can form, and a topological classification of stable Fermi surfaces of any dimension has recently been developed [13, 16].

A promising class of materials in which to search for topological systems are noncentrosymmetric superconductors (NCS). The absence of bulk inversion symmetry in these compounds has two important consequences: it leads to a strong momentum-antisymmetric spin-orbit coupling and it permits the existence of mixed-parity pairing states with both singlet and triplet gaps present [17]. These exotic superconducting properties have inspired a strong research effort [18], and many examples of unconventional superconductivity in NCS have been reported, e.g., $CePt_3Si$ [19], $CeRhSi_3$ [20], $CeIrSi_3$ [21], Li_2Pt_3B [22], Y_2C_3 [23] and $BiPd$ [24]. More recently, much attention has been focused on the possible nontrivial topology of NCS [6, 9, 10, 11, 12, 13, 25, 26, 27, 28, 29, 30, 31, 32]. Specifically, the BCS Hamiltonian of an NCS belongs to class DIII of the Altland-Zirnbauer classification scheme. In two dimensions, gapped DIII systems may be topologically nontrivial and possess a nonzero $\mathbb{Z}_2$ topological number. An example of such a state is given by the NCS with Rashba spin-orbit coupling, s-wave form factor of the gap, and majority-triplet pairing [25, 26, 27, 28]. As shown in figure 1(a), the edge spectrum possesses helically dispersing subgap states with Majorana zero modes [26, 29, 33, 34], as required by the bulk-boundary correspondence. In analogy to a quantum spin Hall insulator, the edge states carry a spin current [29, 34, 35]. Increasing the strength of the singlet pairing ultimately leads to a sign change of the negative-helicity gap, which marks the transition into a state with trivial topology [27]. The edge spectrum of this state does not display any subgap states.

It is likely that many NCS are characterized by rather strong interactions, which may lead to higher orbital-angular-momentum pairing states [36], e.g., the modulation of the gaps by a d_{xy}-wave form factor as shown in figure 1(b). Because of the presence of gap nodes, it is not possible to define a quantized global topological number for such an NCS. This NCS nevertheless also displays edge states with nontrivial topology. Every point in the (lm) edge Brillouin zone not lying on a projected gap node may be regarded as the edge of a fully gapped one-dimensional Hamiltonian in Altland-Zirnbauer class AIII. This allows the definition of a momentum-dependent winding number $W_{(lm)}$, which can only change across projected gap nodes [9, 10]. In the case of the (10) edge shown in figure 1(b), the winding number $W_{(10)}$ evaluates to ± 1 for k_y between the projected edges of the spin-orbit-split Fermi surfaces. By the bulk-boundary correspondence for the one-dimensional class AIII Hamiltonian, it follows
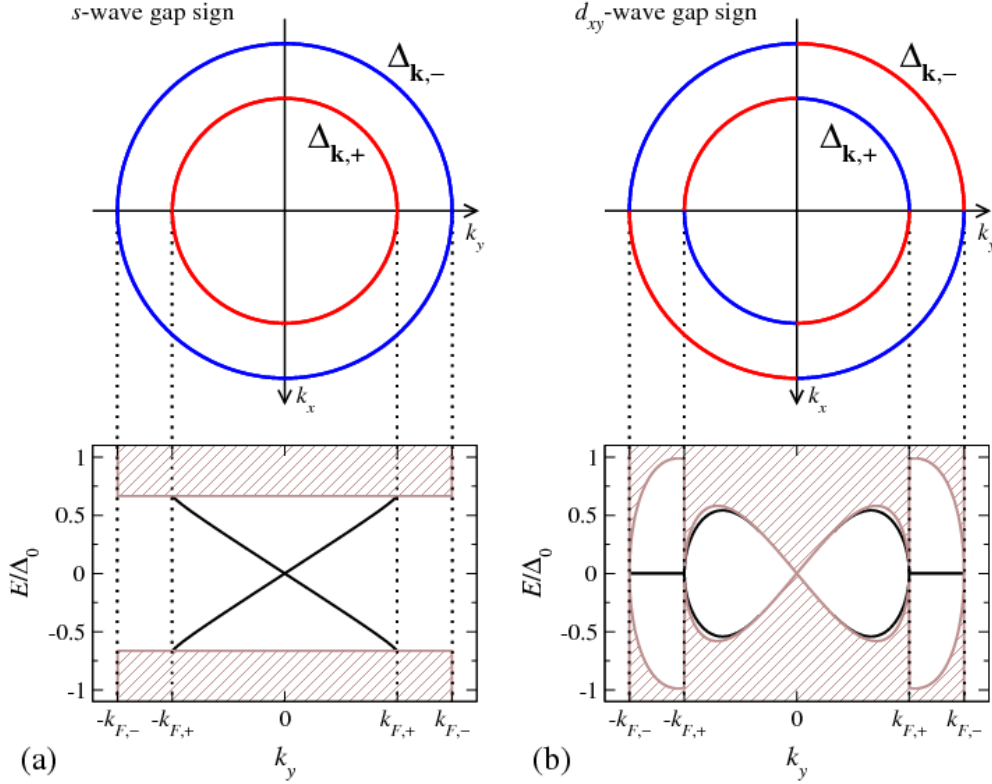
Figure 1.   The relationship of the bulk gap structure to the (10) edge states of an NCS with (a) s-wave and (b) d_{xy}-wave form factors in a majority-triplet state. At the top of the figure we show the variation of the sign of the positive- and negative-helicity gaps, $\Delta_{\mathbf{k},+}$ and $\Delta_{\mathbf{k},-}$ respectively, about the spin-orbit split Fermi surfaces. Here red (blue) indicates positive (negative) sign, and we assume that the positive-helicity (negative-helicity) Fermi surface is circular with Fermi wavevector $k_{F,+}$ ($k_{F,-}$). Below we show the spectrum at the (10) edge for singlet-triplet parameter $q = 0.25$, where black lines indicate edge states while the brown shaded region is the projection of the continuum onto the one-dimensional edge Brillouin zone.

that there is a nondegenerate zero-energy flat band at these momenta [9, 30, 31]. The d_{xy}-wave form factor is crucial here, as one may show that these states can only form when there is a sign difference between the gap on the forwards- and backwards-facing parts of the Fermi surface [11, 32]. As such, these states are present for both majority-triplet and majority-singlet pairing states. In contrast, the edge states at momenta k_y lying between the projected edges of the positive-helicity Fermi surface depend upon the relative strength of the singlet and triplet gap: for a majority-triplet state there are topologically trivial dispersing states, whereas for majority-singlet pairing there are doubly degenerate zero-energy states with $W_{(10)} = \pm 2$.

Much attention has been paid to the spin structure of the edge states of an NCS [29, 34, 35], as the surface spin current can be understood in terms of the polarization of the *electronlike* part of the edge state wavefunctions.   We have recently shown [37] that the edge states of an NCS typically also have rather strong

total spin polarization, which consists of contributions from the electronlike and holelike components of the wavefunctions. Like the polarization of the electronlike wavefunction components [29, 34, 35], the total spin polarization is odd in the edge momentum as required by time-reversal symmetry, and depends on both the spin-orbit coupling and the relative strength of the singlet and triplet pairing. On the other hand, the total spin polarization can be rather different from the electronlike spin polarization, and it is the total polarization that couples to an external exchange field. In particular, we have demonstrated that the topologically protected zero-energy flat bands characteristic of the NCS with d_{xy}-wave form factor have particularly strong total spin polarization. Coupling to an exchange field therefore gives opposite energy shifts to these flat bands on either side of the edge Brillouin zone, hence generating an imbalance between the integrated spectral density at these two momenta. This causes the appearance of a finite edge current, which depends rather strongly on the orientation of the exchange field, and shows a remarkable singular dependence on the exchange-field strength at zero temperature. In contrast, the absence of the flat bands for an NCS with s-wave form factor leads to a very weak edge current due to the interplay between the spin-orbit coupling and the spin polarization induced by the exchange field.

The analysis in Ref. [37] was performed for an NCS strip in contact with a ferromagnetic *insulator* at one edge. The strip was described by a lattice model with an exchange field applied to the sites on one edge. Note that applying an exchange field to the entire NCS also leads to an energy shift of the edge states [13, 31, 38] but additionally distorts the Fermi surfaces in a way which is inconsistent with a zero-momentum pairing state [39, 40]. In the present paper we consider an NCS in proximity contact with a bulk *metallic* ferromagnet (FM), with each phase occupying a half-space and treated in the continuum limit. We note that such an NCS-FM heterostructure has been studied by other authors [41, 42], but they only address the proximity effect on the FM which does not concern us here. A fundamental difference between Ref. [37] and the present work is that the direct coupling between the edge states and the exchange field in the former is absent in the latter. While the edge states remain well-defined when an exchange field is applied to the edge layer [37], for the half-space continuum system tunneling into the bulk states of the FM gives them a finite lifetime and hence turns them into broadened resonances. One of our main goals is to understand how these differences affect the edge current. To accomplish this, we utilize a quasiclassical technique to express the interface current in terms of Andreev reflection processes. The quasiclassical technique also has the advantage of being able to treat realistically small superconducting gaps, whereas the exact-diagonalization approach used in Ref. [37] requires rather large gaps to avoid finite-size artifacts. We perform a systematic study of the current's dependence on the temperature, the pairing state of the NCS, and the exchange field in the FM. For the d_{xy}-wave form factor, we find that the key features of the interface current are robust to the additional complications of a metallic FM. In contrast, the results for the s-wave form factor show that the broadening of the subgap interface states leads to qualitatively different behaviour of the current at low temperatures. We use the close relationship between the current and the interface local density of states to understand the origin of the current, and show how it reflects the topology of the NCS.

Our paper is organized as follows. We commence in section 2 with the theoretical description of the system, including the construction of the scattering wavefunctions,
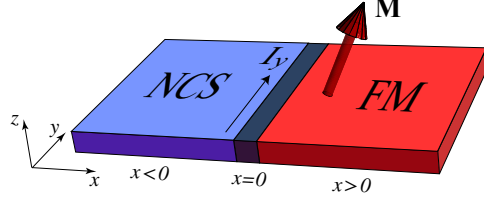
Figure 2. Schematic diagram of the NCS-FM heterostructure considered in this work. The NCS and FM occupy the $x < 0$ and $x > 0$ half spaces, respectively, and are separated by an insulating barrier. The magnetization **M** of the FM is allowed to point in any direction. In general, we find that an interface current I_y is present in the NCS as indicated by the black arrow.

an ansatz for the Green's function in the NCS and the derivation of the current. In section 3, we present and discuss the results for the s-wave and d_{xy}-wave gap form factors. This is followed in section 4 by a discussion of possible experiments. We summarize our work in section 5.

2. Theory

We study a planar junction between a bulk NCS and a metallic FM separated by a thin insulating barrier, see figure 2. The Hamiltonian is written as

$$H = \int d^2r\, \underline{\Psi}^\dagger(\mathbf{r})\check{H}(\mathbf{r})\underline{\Psi}(\mathbf{r}) = \int d^2r\, \underline{\Psi}^\dagger(\mathbf{r}) \begin{pmatrix} \hat{H}_0(\mathbf{r}) & \hat{\Delta}(\mathbf{r}) \\ \hat{\Delta}^\dagger(\mathbf{r}) & -\hat{H}_0^T(\mathbf{r}) \end{pmatrix} \underline{\Psi}(\mathbf{r}) \tag{1}$$

where $\underline{\Psi}(\mathbf{r})$ is the Nambu spinor of field operators. We also introduce the notation of the hat and the caron (inverted hat) to denote 2×2 matrices in spin space and 4×4 matrices in Nambu-spin space, respectively. The noninteracting Hamiltonian is

$$\hat{H}_0(\mathbf{r}) = \left[-\frac{\hbar^2 \boldsymbol{\nabla}^2}{2m} - E_F + U\delta(x) \right] \hat{\sigma}_0 - \mu_B \Theta(x) \mathbf{H}_{\text{ex}} \cdot \hat{\boldsymbol{\sigma}}$$
$$+ \frac{\lambda}{2} \left\{ \Theta(-x) \left[(-i\boldsymbol{\nabla}) \times \mathbf{e}_z \right] \cdot \hat{\boldsymbol{\sigma}} + \left[(-i\boldsymbol{\nabla}) \times \mathbf{e}_z \right] \cdot \hat{\boldsymbol{\sigma}} \Theta(-x) \right\} . \tag{2}$$

For simplicity, we assume that the effective mass m and Fermi energy E_F are the same in the NCS and FM. The insulating layer separating the NCS and FM is modeled as a δ-function barrier of strength U. In the NCS there is a Rashba spin-orbit coupling λ, while the FM is characterized by an exchange field $\mathbf{H}_{\text{ex}} = |\mathbf{H}_{\text{ex}}| (\cos\eta\sin\zeta\, \mathbf{e}_x + \sin\eta\sin\zeta\, \mathbf{e}_y + \cos\zeta\, \mathbf{e}_z)$; note that the spatially-dependent spin-orbit coupling in (2) is written in symmetrized and thus Hermitian form. The spin degeneracy of the circular Fermi surfaces is therefore lifted in both the NCS and the FM: in the NCS we have positive-helicity $(+)$ and negative-helicity $(-)$ Fermi surfaces with radii $k_{F,\pm} = k_F(\sqrt{1 + \widetilde{\lambda}^2} \mp \widetilde{\lambda})$ where $\widetilde{\lambda} = \lambda k_F/(2E_F)$ and $k_F = \sqrt{2mE_F/\hbar^2}$; similarly, in the FM the Fermi wavevectors for the majority $(\uparrow)$ and minority spin $(\downarrow)$ Fermi surfaces are $k_{F,\uparrow(\downarrow)} = k_F\sqrt{1 + (-)h_{\text{ex}}}$, where $h_{\text{ex}} = \mu_B|\mathbf{H}_{\text{ex}}|/E_F$. The minority Fermi surface disappears at $h_{\text{ex}} = 1$, and the FM becomes a half-metal.

The gap matrix is

$$\hat{\Delta}(\mathbf{r}) = \Theta(-x)\, f(\boldsymbol{\nabla})\, i[\psi\hat{\sigma}_0 + \mathbf{d} \cdot \hat{\boldsymbol{\sigma}}]\, \hat{\sigma}_y \tag{3}$$

where $\psi = \Delta(T)q$ and $\mathbf{d} = (-i\boldsymbol{\nabla} \times \mathbf{e}_z)\Delta(T)(1-q)/k_F$ are the singlet and triplet pairing fields, respectively [17]. The parameter q tunes the NCS from purely spin-triplet ($q = 0$) to purely spin-singlet ($q = 1$) pairing. The gap magnitude $\Delta(T)$ is assumed to have weak-coupling temperature dependence, with $\Delta(T = 0) = \Delta_0$. The form factor $f(\boldsymbol{\nabla})$ models different orbital-angular-momentum pairing states: $f(\boldsymbol{\nabla}) = 1$ for an NCS with $(s+p)$-wave pairing symmetry; and $f(\boldsymbol{\nabla}) = -2\partial_x\partial_y/k_F^2$ for a $(d_{xy}+p)$-wave pairing state. Writing the gap function in momentum space and adopting the helicity basis, there is only intra-helicity pairing with distinct gaps $\Delta_{\mathbf{k},\pm} = f(i\mathbf{k})(\psi_{\mathbf{k}} \pm |\mathbf{d_k}|)$ on the spin-split Fermi surfaces. For the circular Fermi surfaces considered here the negative-helicity gap vanishes at $q = q_c$ with $q_c = k_{F,-}/(k_{F,-} + k_F) \approx 0.55$, which may be regarded as the boundary between majority-triplet ($q < q_c$) and majority-singlet ($q > q_c$) pairing states.

2.1. Scattering wavefunction

The Bogoliubov-de Gennes equation for the quasiparticle states $\psi(\mathbf{r})$ with energy E is written in Nambu-spin space as

$$\check{H}(\mathbf{r})\psi(\mathbf{r}) = E\psi(\mathbf{r}). \qquad (4)$$

We solve (4) for the scattering states. As an example, the wavefunction for a ν-helicity electronlike quasiparticle with wavevector $\mathbf{k}_\nu = (k_{\nu,x}, k_y)$ incident upon the FM from the NCS is given by

$$
\begin{aligned}
\psi_{e\nu}(k_y, x) = \Theta(-x)e^{ik_y y}\Big(&\phi^{\text{NCS}}_{e,\mathbf{k}_\nu,\nu} e^{ik_{\nu,x}x} \\
&+ \sum_{\nu'=\pm} \Big\{ \Big[a^e_{\nu\nu'}\phi^{\text{NCS}}_{h,\mathbf{k}_{\nu'},\nu'} e^{ik_{\nu',x}x} + b^e_{\nu\nu'}\phi^{\text{NCS}}_{e,\widetilde{\mathbf{k}}_{\nu'},\nu'} e^{-ik_{\nu',x}x} \Big] \Theta(k_{F,\nu'} - |k_y|) \\
&+ \Big[a^e_{\nu\nu'}\widetilde{\phi}^{\text{NCS}}_{h,k_y,\nu'} e^{\kappa_{\nu'}x} + b^e_{\nu\nu'}\widetilde{\phi}^{\text{NCS}}_{e,k_y,\nu'} e^{\kappa_{\nu'}x} \Big] \Theta(|k_y| - k_{F,\nu'}) \Big\} \Big) \\
&+ \Theta(x)e^{ik_y y} \sum_{\sigma=\uparrow,\downarrow} \Big\{ \Big[c^e_{\nu\sigma}\phi^{\text{FM}}_{h,\sigma} e^{-ik_{\sigma,x}x} + d^e_{\nu\sigma}\phi^{\text{FM}}_{e,\sigma} e^{ik_{\sigma,x}x} \Big] \Theta(k_{F,\sigma} - |k_y|) \\
&+ \Big[c^e_{\nu\sigma}\phi^{\text{FM}}_{h,\sigma} e^{-\kappa_\sigma x} + d^e_{\nu\sigma}\phi^{\text{FM}}_{e,\sigma} e^{-\kappa_\sigma x} \Big] \Theta(|k_y| - k_{F,\sigma}) \Big\}. \qquad (5)
\end{aligned}
$$

For $x < 0$, the ansatz describes Andreev reflection of ν'-helicity holelike quasiparticles with wavevector $\mathbf{k}_{\nu'} = (k_{\nu',x}, k_y)$ and reflection probability amplitude $a^e_{\nu\nu'}$ and the normal reflection of ν'-helicity electronlike quasiparticles with wavevector $\widetilde{\mathbf{k}}_{\nu'} = (-k_{\nu',x}, k_y)$ and probability amplitude $b^e_{\nu\nu'}$. For $x > 0$, the quasiparticle is transmitted as a spin-σ hole with wavevector $\widetilde{\mathbf{k}}_\sigma = (-k_{\sigma,x}, k_y)$ and amplitude $c^e_{\nu\sigma}$ or as a spin-σ electron with wavevector $\mathbf{k}_\sigma = (k_{\sigma,x}, k_y)$ and amplitude $d^e_{\nu\sigma}$, respectively. Here we have made the standard assumption of $E \ll E_F$ and thereby approximate the magnitude of the wavevectors for electrons and holes to be equal; relaxing this approximation is not expected to qualitatively alter our results. Note also that the momentum k_y parallel to the interface is a good quantum number due to translational invariance along the y-axis. If $|k_y|$ is larger than the Fermi momentum in a given scattering channel, only evanescent solutions in this channel are possible. These solutions are characterized by an inverse decay length into the bulk NCS (FM) of κ_ν^{-1} (κ_σ^{-1}).

The wave function (5) is expressed in terms of the spinors for the NCS and FM. In the FM, the spinors for electrons (e) and holes (h) are

$$\phi_{e,\uparrow}^{\mathrm{FM}} = \frac{1}{\sqrt{2}} \left(e^{-i\eta} \cos \frac{\zeta}{2}, \, \sin \frac{\zeta}{2}, \, 0, \, 0 \right)^T \tag{6a}$$

$$\phi_{e,\downarrow}^{\mathrm{FM}} = \frac{1}{\sqrt{2}} \left(-e^{-i\eta} \sin \frac{\zeta}{2}, \, \cos \frac{\zeta}{2}, \, 0, \, 0 \right)^T \tag{6b}$$

$$\phi_{h,\uparrow}^{\mathrm{FM}} = \frac{1}{\sqrt{2}} \left(0, \, 0, \, e^{i\eta} \cos \frac{\zeta}{2}, \, \sin \frac{\zeta}{2} \right)^T \tag{6c}$$

$$\phi_{h,\downarrow}^{\mathrm{FM}} = \frac{1}{\sqrt{2}} \left(0, \, 0, \, -e^{i\eta} \sin \frac{\zeta}{2}, \, \cos \frac{\zeta}{2} \right)^T . \tag{6d}$$

In the NCS, the spinors for electronlike and holelike quasiparticles with momentum $\mathbf{k}$ and helicity ν are given by

$$\phi_{e,\mathbf{k},\nu}^{\mathrm{NCS}} = \frac{1}{\sqrt{2}} \left(u_{\mathbf{k},\nu}, \, -\nu i e^{i\theta} u_{\mathbf{k},\nu}, \, \nu i e^{i\theta} s_{\mathbf{k},\nu} v_{\mathbf{k},\nu}, \, s_{\mathbf{k},\nu} v_{\mathbf{k},\nu} \right)^T \tag{7a}$$

$$\phi_{h,\mathbf{k},\nu}^{\mathrm{NCS}} = \frac{1}{\sqrt{2}} \left(v_{\mathbf{k},\nu}, \, -\nu i e^{i\theta} v_{\mathbf{k},\nu}, \, \nu i e^{i\theta} s_{\mathbf{k},\nu} u_{\mathbf{k},\nu}, \, s_{\mathbf{k},\nu} u_{\mathbf{k},\nu} \right)^T \tag{7b}$$

where $\mathbf{k} = k_{F,\nu}(\cos\theta, \sin\theta)$, $s_{\mathbf{k},\nu} = \mathrm{sgn}(\Delta_{\mathbf{k},\nu})$ and

$$u_{\mathbf{k},\nu} = \sqrt{\frac{E + \Omega_{\mathbf{k},\nu}}{2E}} \tag{8a}$$

$$v_{\mathbf{k},\nu} = \sqrt{\frac{E - \Omega_{\mathbf{k},\nu}}{2E}} \tag{8b}$$

$$\Omega_{\mathbf{k},\nu} = \sqrt{E^2 - \Delta_{\mathbf{k},\nu}^2} . \tag{8c}$$

Evanescent solutions in the NCS are characterized by the spinors

$$\widetilde{\phi}_{e,k_y,\nu}^{\mathrm{NCS}} = \frac{1}{\sqrt{2}} \left(1, \, \nu \frac{k_y - \kappa_\nu}{k_{F,\nu}}, \, 0, \, 0 \right)^T \tag{9a}$$

$$\widetilde{\phi}_{h,k_y,\nu}^{\mathrm{NCS}} = \frac{1}{\sqrt{2}} \left(0, \, 0, \, 1, \, -\nu \frac{k_y + \kappa_\nu}{k_{F,\nu}} \right)^T \tag{9b}$$

where $\kappa_\nu = \sqrt{k_y^2 - k_{F,\nu}^2}$.

The reflection and transmission amplitudes in (5) are determined from the boundary conditions obeyed by the wave function at the NCS-FM interface. Firstly, we require that the wavefunction is continuous at the interface

$$\psi_{e\nu}(k_y, x = 0^-) = \psi_{e\nu}(k_y, x = 0^+). \tag{10}$$

To ensure the conservation of probability [43], the wavefunction must also obey the condition

$$\partial_x \psi_{e\nu}(k_y, x)|_{x=0^+} - \partial_x \psi_{e\nu}(k_y, x)|_{x=0^-} = \hat{\sigma}_0 \otimes \left(Z k_F \hat{\sigma}_0 - i \widetilde{\lambda} k_F \hat{\sigma}_y \right) \psi_{e\nu}(k_y, x = 0) \tag{11}$$

where $Z = U k_F / E_F$ is a dimensionless constant characterizing the strength of the insulating barrier. These conditions yield eight coupled equations for the probability amplitudes.

The calculation for a ν-helicity *holelike* quasiparticle incident on the interface proceeds analogously. The reflection and transmission coefficients in this case are denoted by a superscript h, i.e., $a_{\nu\nu'}^h$, $b_{\nu\nu'}^h$, etc.

2.2. The Green's function

Generalizing the method of Refs. [44, 45, 46, 47], we obtain the following expression for the retarded Green's function $\check{G}^r_{\mathrm{NCS}}(\mathbf{r}, \mathbf{r}'; E)$ in the NCS as a 4×4 matrix in Nambu-spin space:

$$
\begin{aligned}
\check{G}^r_{\mathrm{NCS}}(\mathbf{r}, \mathbf{r}'; E) &= \int \frac{dk_y}{2\pi} \, \check{G}^r_{\mathrm{NCS}}(k_y, x, x'; E) e^{ik_y(y-y')} \\
&= \int \frac{dk_y}{2\pi} \sum_{\nu,\nu'} \frac{m}{i\hbar^2 \sqrt{1+\widetilde{\lambda}^2} \, k_F \cos\theta_{\nu'}} \, \frac{E}{\Omega_{k_y,\nu'}} \Theta(k_{F,\nu} - |k_y|) \Theta(k_{F,\nu'} - |k_y|) \\
&\quad \times \Bigg[\Big\{ \delta_{\nu,\nu'} \phi^{\mathrm{NCS}}_{e,\mathbf{k},\nu} e^{i(k_{\nu,x}+q_\nu)x} + b^e_{\nu'\nu} \phi^{\mathrm{NCS}}_{e,\widetilde{\mathbf{k}},\nu} e^{-i(k_{\nu,x}+q_\nu)x} \\
&\quad + a^e_{\nu'\nu} \phi^{\mathrm{NCS}}_{h,\mathbf{k},\nu} e^{i(k_{\nu,x}-q_\nu)x} \Big\} \big(\phi^{\mathrm{NCS}}_{e,\mathbf{k},\nu'}\big)^\dagger e^{-i(k_{\nu',x}+q_{\nu'})x'} \\
&\quad + \Big\{ \delta_{\nu,\nu'} \phi^{\mathrm{NCS}}_{h,\widetilde{\mathbf{k}},\nu} e^{-i(k_{\nu,x}-q_\nu)x} + b^h_{\nu'\nu} \phi^{\mathrm{NCS}}_{h,\mathbf{k},\nu} e^{i(k_{\nu,x}-q_\nu)x} \\
&\quad + a^h_{\nu'\nu} \phi^{\mathrm{NCS}}_{e,\widetilde{\mathbf{k}},\nu} e^{-i(k_{\nu,x}+q_\nu)x} \Big\} \big(\phi^{\mathrm{NCS}}_{h,\widetilde{\mathbf{k}},\nu'}\big)^\dagger e^{i(k_{\nu',x}-q_{\nu'})x'} \Bigg] e^{ik_y(y-y')} .
\end{aligned} \tag{12}
$$

We present only the result for $x' < x < 0$, which is sufficient to obtain all quantities of interest; the Green's function for $x < x' < 0$ has similar form. In constructing (12), we assume that $|\Delta_{\mathbf{k},\nu}| = |\Delta_{\widetilde{\mathbf{k}},\nu}| = \Delta_{k_y,\nu}$ (valid for the gaps considered here), and we hence introduce the notation $\Omega_{\mathbf{k},\nu} = \Omega_{k_y,\nu}$. For the Green's function it is necessary to include the energy-dependent corrections to the electron- and hole-wavevectors, i.e., $k_{e,\nu,x} \approx k_{\nu,x} + q_\nu$ and $k_{h,\nu,x} \approx k_{\nu,x} - q_\nu$, where

$$
q_\nu = \frac{m\Omega_{k_y,\nu}}{\hbar^2 \sqrt{1+\widetilde{\lambda}^2} \, k_F \cos\theta_\nu} . \tag{13}
$$

Note that we neglect contributions from scattering into evanescent states in the Green's function ansatz, as enforced by the step functions in (12).

2.3. Transverse interface current

The currents are derived from the continuity equation. The charge-density operator $\hat{\rho}(\mathbf{r}) = -e\sum_\sigma \hat{\psi}^\dagger_\sigma(\mathbf{r})\hat{\psi}_\sigma(\mathbf{r})$ obeys the Heisenberg equation of motion

$$
\frac{\partial}{\partial t} \hat{\rho}(\mathbf{r}) = \frac{1}{i\hbar}[\hat{\rho}(\mathbf{r}), \hat{H}] = \frac{1}{i\hbar}\Big([\hat{\rho}(\mathbf{r}), \hat{H}_N] + [\hat{\rho}(\mathbf{r}), \hat{H}_P]\Big) = -\boldsymbol{\nabla}\cdot\hat{\mathbf{J}}_e(\mathbf{r}) - \boldsymbol{\nabla}\cdot\hat{\mathbf{J}}_s(\mathbf{r}) \tag{14}
$$

where $\hat{H}_N$ and $\hat{H}_P$ are the normal-state and pairing Hamiltonians, respectively. The commutators of these Hamiltonians with the charge-density operator correspond to the divergence of the so-called electronic and source current density operators, $\hat{\mathbf{J}}_e(\mathbf{r})$ and $\hat{\mathbf{J}}_s(\mathbf{r})$, respectively [46, 47]. The total current density is obtained by calculating the expectation value $\mathbf{J}(\mathbf{r}) = \langle \hat{\mathbf{J}}_e(\mathbf{r}) + \hat{\mathbf{J}}_s(\mathbf{r}) \rangle$. Only the electronic term contributes to the transverse current.

After a lengthy calculation, the y-component of the charge current density in the NCS can be expressed in terms of the retarded Green's function as

$$
\begin{aligned}
J_y(x) &= \frac{1}{\beta} \sum_{i\omega_n} \lim_{\mathbf{r}'\to\mathbf{r}} \mathrm{Tr}\left\{ \left(\frac{ie\hbar}{4m}\left[\frac{\partial}{\partial y} - \frac{\partial}{\partial y'}\right] - \frac{e\lambda}{\hbar}\check{S}_x \right) \check{G}^r_{\mathrm{NCS}}(\mathbf{r},\mathbf{r}'; E) \right\}\bigg|_{E\to i\omega_n} \\
&= -\frac{1}{\beta}\sum_{i\omega_n} \int \frac{dk_y}{2\pi} \mathrm{Tr}\left\{ \left(\frac{e\hbar k_y}{2m} + \frac{e\lambda}{\hbar}\check{S}_x \right) \check{G}^r_{\mathrm{NCS}}(k_y, x, x; E) \right\}\bigg|_{E\to i\omega_n} \tag{15}
\end{aligned}
$$

where $\check{S}_x = \mathrm{diag}(\hat{\sigma}_x, -\hat{\sigma}_x)$. Note that the first term in the brackets in (15) originates from the kinetic energy, while the second term is due to the spin-orbit coupling. The current density can equivalently be written as

$$J_y(x) = -\int \frac{dk_y}{2\pi} \int dE \left\{ \frac{e\hbar}{2m} k_y \rho(E, k_y, x) + \frac{e\lambda}{\hbar} \rho^x(E, k_y, x) \right\} n_F(E) \tag{16}$$

where $n_F(E)$ is the Fermi distribution function and

$$\rho(E, k_y, x) = -\frac{1}{4\pi} \mathrm{Im}\left(\mathrm{Tr}\left\{ \check{G}^r_{\mathrm{NCS}}(k_y, x, x; E) \right\}\right) \tag{17}$$

$$\rho^x(E, k_y, x) = -\frac{\hbar}{4\pi} \mathrm{Im}\left(\mathrm{Tr}\left\{ \check{G}^r_{\mathrm{NCS}}(k_y, x, x; E) \check{S}_x \right\}\right) \tag{18}$$

are the energy- and momentum-resolved local density of states (LDOS) and x-spin-resolved LDOS at distance x from the interface, respectively. Although (16) is of limited calculational value, it is useful for interpreting our results. In particular, we note that the interface current depends on the reconstructed electronic structure at the NCS-FM interface only through these quantities.

From examination of the Green's function, we determine that four distinct scattering processes contribute to $J_y(x)$: intra- and inter-helicity normal reflection, and intra- and inter-helicity Andreev reflection. All these contributions show exponential decay into the bulk NCS on the scale of the coherence length $\xi_0 = \hbar v_F/(\pi\Delta_0)$. The interface current density due to normal reflection and inter-helicity Andreev reflection processes are, however, further modulated by rapidly oscillating factors with the length scales $\sim(2k_F)^{-1}$ and $\sim(2\widetilde{\lambda}k_F)^{-1}$, respectively. As these length scales are much shorter than ξ_0, the total current contributed by these processes is negligible and we henceforth ignore them. We thus find the total interface current I_y in the NCS to be

$$\begin{aligned} I_y &= \int_{-\infty}^0 dx\, J_y(x) \\ &= -\frac{e\hbar}{8\pi m}\frac{1}{\beta}\sum_{i\omega_n}\int dk_y\, k_y \sum_\nu \Theta(k_{F,\nu} - |k_y|)\frac{k_{F,\overline{\nu}}}{k_{F\nu}}\left(\frac{\Delta_{k_y,\nu}}{\Omega_{k_y,\nu}^2}\left(a_{\nu\nu}^h + a_{\nu\nu}^e\right)\right)\bigg|_{E \to i\omega_n}. \end{aligned} \tag{19}$$

In deriving (19), we find that the current in the ν-helicity sector contributed by the spin-orbit coupling is exactly $2\nu\widetilde{\lambda}/k_{F,\nu}$ times that from the kinetic energy.

A similar expression to (15) can be derived for the interface charge current density in the FM in terms of the FM Green's function $\check{G}^r_{\mathrm{FM}}(\mathbf{r}, \mathbf{r}'; E)$. As in the NCS, the Green's function of the FM includes terms due to normal and Andreev reflection at the interface. Due to the absence of a pairing potential in the FM region, however, the latter processes only appear in the off-diagonal elements of the Green's function, and as such they give vanishing contribution to the trace in the expression for the interface current. Since the remaining contribution of normal reflection to the charge current density oscillates on the scale of the inverse Fermi momenta, we expect the integrated current in the FM to be negligible compared to that in the NCS.

3. Results

We find that an interface current appears in the NCS for a FM with magnetization components along the x- or z-axes, and reverses direction with the magnetization. In agreement with Ref. [37], there is no current for a y-polarized FM. In the following

we will consider the two cases of a magnetic moment pointing along the positive x- and z-axes. We present results only for spin-orbit coupling strength $\widetilde{\lambda} = 0.2$ and barrier strength $U = 3E_F/k_F$. Note that the symbols in the plots of the currents are included to distinguish the curves and do not represent the only data points. In performing the Matsubara sum we utilize a frequency cutoff of $100\Delta_0$. Our finite-temperature analysis is extended to zero temperature by replacing the Matsubara summation in (19) by an integral over the imaginary frequency axis. We express the current in units of $eE_F/2\pi\hbar$, which is twice the magnitude of the edge current of a chiral p-wave superconductor [48, 49].

3.1. (s+p)-wave pairing state

In figure 3 we plot the total interface current in the NCS for the $(s+p)$-wave pairing state as a function of temperature [panels (a) and (b)], singlet-triplet parameter q [panels (c) and (d)], and exchange-field strength h_{ex} [panels (e) and (f)]. For weak to moderate exchange-field strengths the magnitude of the current in the $(s+p)$-wave NCS is always very small compared to the edge current of a chiral p-wave superconductor. At low temperatures it converges to a value which is weakly dependent on q in both the topologically trivial ($q > q_c$) and nontrivial ($q < q_c$) states, but has markedly larger magnitude in the latter. Just on the nontrivial side of the topological transition, we see that the current increases rather steeply at low temperature, note, e.g., the $q = 0.5$ curves in panels (a) and (b). Plotting the zero-temperature current as a function of q reveals a step discontinuity at $q = q_c$, as seen in panels (c) and (d). Although the current in the topologically nontrivial NCS is roughly three times larger for a FM polarized along the z-axis than along the x-axis, in the topologically trivial state the two magnetization directions give comparable results. The current shows typical linear-response behaviour for small exchange-field strengths h_{ex}. Approaching the half-metal limit $h_{\text{ex}} = 1$, we observe that the zero-temperature current appears to saturate for the x-polarized FM, but for a magnetization along the z-axis the current increases super-linearly with the exchange field.

Insight into the origin of the current can be gained by examining the momentum-resolved quantity $I_y(k_y)$, defined as the even part of the k_y integrand in (19). In figure 4 we plot the evolution of $I_y(k_y)$ with the singlet-triplet parameter q [panels (a), (b)] and the temperature [panels (c), (d)]. This reveals that the states at $|k_y| < k_{F,+}$ are responsible for the sharp drop in the current at $q = q_c$, and also for the large disparity between the currents for the x- and z-polarized FM in the topologically nontrivial case. In contrast, the momentum-resolved current at $k_{F,+} < |k_y| < k_{F,-}$ is almost independent of the singlet-triplet parameter for $T = 0.1\,T_c$, except very close to $q = q_c$, where the negative-helicity gap closes; indeed, in panels (a) and (b) the curves for $q = 1$, 0.75 and 0.25 are obscured by the $q = 0$ result. At zero temperature all curves for $q \neq q_c$ are identical for $k_{F,+} < |k_y| < k_{F,-}$ (not shown). This can be understood by noting that due to the absence of positive-helicity states, varying q only scales the energy dependence of the Andreev reflection coefficients by the changing negative-helicity gap, which is irrelevant at zero temperature. On the other hand, the absence of the negative-helicity gap at $q = q_c$ completely suppresses Andreev reflection, and thus there is vanishing current. Note also that the current at $k_{F,+} < |k_y| < k_{F,-}$ is comparable for the x- and z-polarizations of the FM.

The most interesting features of the current in the $(s+p)$-wave NCS are the zero-temperature step discontinuity at the topological transition ($q = q_c$) and the
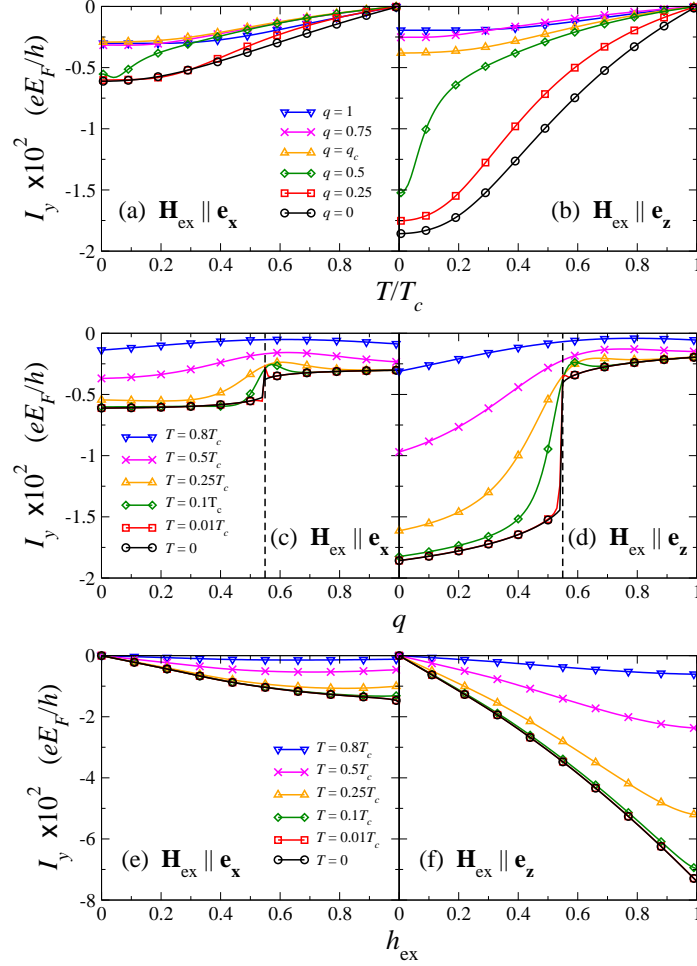
Figure 3. Interface currents in the $(s+p)$-wave NCS for a FM polarized along the x-axis (left column) and z-axis (right column). Current as a function of: (a), (b) temperature T at exchange-field strength $h_{ex} = \mu_B |\mathbf{H}_{ex}|/E_F = 0.3$; (c), (d) singlet-triplet parameter q for exchange-field strength $h_{ex} = 0.3$, where the vertical dashed line indicates the critical value q_c; (e), (f) exchange-field strength h_{ex} for singlet-triplet parameter $q = 0.25$.

much larger current for the majority-triplet pairing state. The momentum-resolved results allow us to associate the jump at $q = q_c$ with a suppression of the current at $|k_y| < k_{F,+}$, which naturally suggests that the enhanced current in the topologically nontrivial state is due to the presence of subgap states. This is also consistent with the sharp low-temperature increase of the current near the closing of the negative-helicity gap at $q = q_c$ (see, e.g., the $q = 0.5$ curves in figures 3(a) and (b)), as the subgap states can only contribute to the current at temperatures less than the minimum gap.

To see how the edge states might carry a current, we first examine the analytically tractable limit of vanishing spin-orbit coupling and a purely triplet gap. In this case the Bogoliubov-de Gennes equation (4) in the NCS splits up into two 2×2
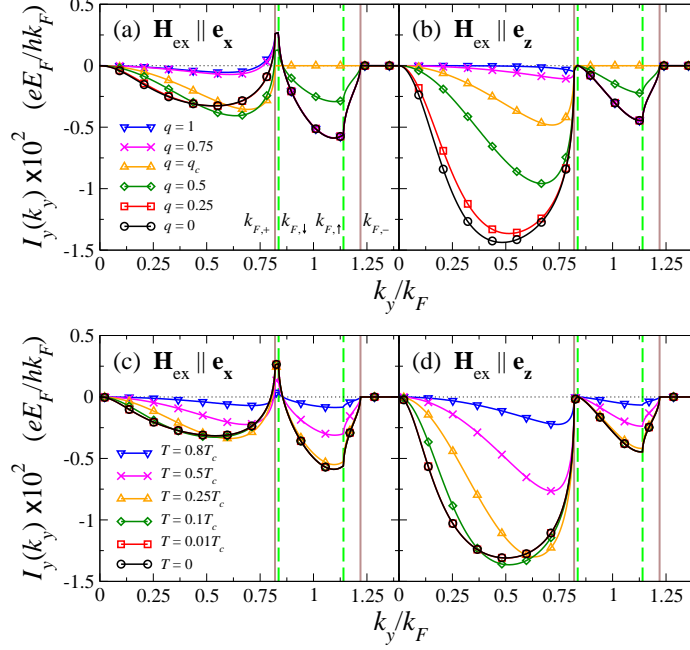
Figure 4. Momentum-resolved interface current in the $(s+p)$-wave NCS for a FM polarized along the x-axis (left column) and z-axis (right column) with exchange-field strength $h_{\text{ex}} = 0.3$. (a), (b): The current for various values of the singlet-triplet parameter q at temperature $T = 0.1\,T_c$. (c), (d): The current for various temperatures T at singlet-triplet parameter $q = 0.25$. In all panels the vertical brown solid (green dashed) lines are the projections of the positive- and negative-helicity Fermi surfaces of the NCS (majority and minority spin Fermi surfaces of the FM), as shown in panel (a).

systems with opposite chiral p-wave gaps, one for each Cooper pair z-spin orientation $s = \pm 1$. At a vacuum edge of this so-called helical superconductor one finds subgap states with dispersion $E_{s=\pm}(k_y) = s\Delta_0 k_y/k_F$ [25, 33, 34]. When placed next to a z-polarized metallic FM, the spin-dependent reflectivity $\mathcal{R}_s(k_y)$ leads to an unequal broadening of these states. In particular, by calculating the poles of the Andreev reflection coefficients, we obtain the energy of the subgap states

$$E_s(k_y) = \Delta_0 \sin\left(\arcsin\frac{sk_y}{k_F} + i\ln\sqrt{\mathcal{R}_s(k_y)}\right). \tag{20}$$

The left- and right-moving subgap states therefore have finite but different lifetimes when $\mathcal{R}_+(k_y) \neq \mathcal{R}_-(k_y) < 1$, and thus appear as resonances of different width in the energy- and momentum-resolved LDOS $\rho(E, k_y, x)$ in the NCS. On the other hand, there is no asymmetry in the spin-degenerate continuum states, i.e., we find that $\rho(E, k_y, x) \neq \rho(E, -k_y, x)$ only for energies $|E| < \Delta_0$. Furthermore, the integrals of the LDOS at k_y and $-k_y$ over the negative-energy states are unequal $\int_{-\Delta_0}^{0} dE\, \rho(E, k_y, x) \neq \int_{-\Delta_0}^{0} dE\, \rho(E, -k_y, x)$, and so from (16) we deduce that there is a finite charge current density in the NCS which is carried entirely by the subgap states. We note that the spin-dependent broadening is not connected to the total polarization of the states, but rather is controlled by the polarization of the electronlike part of the
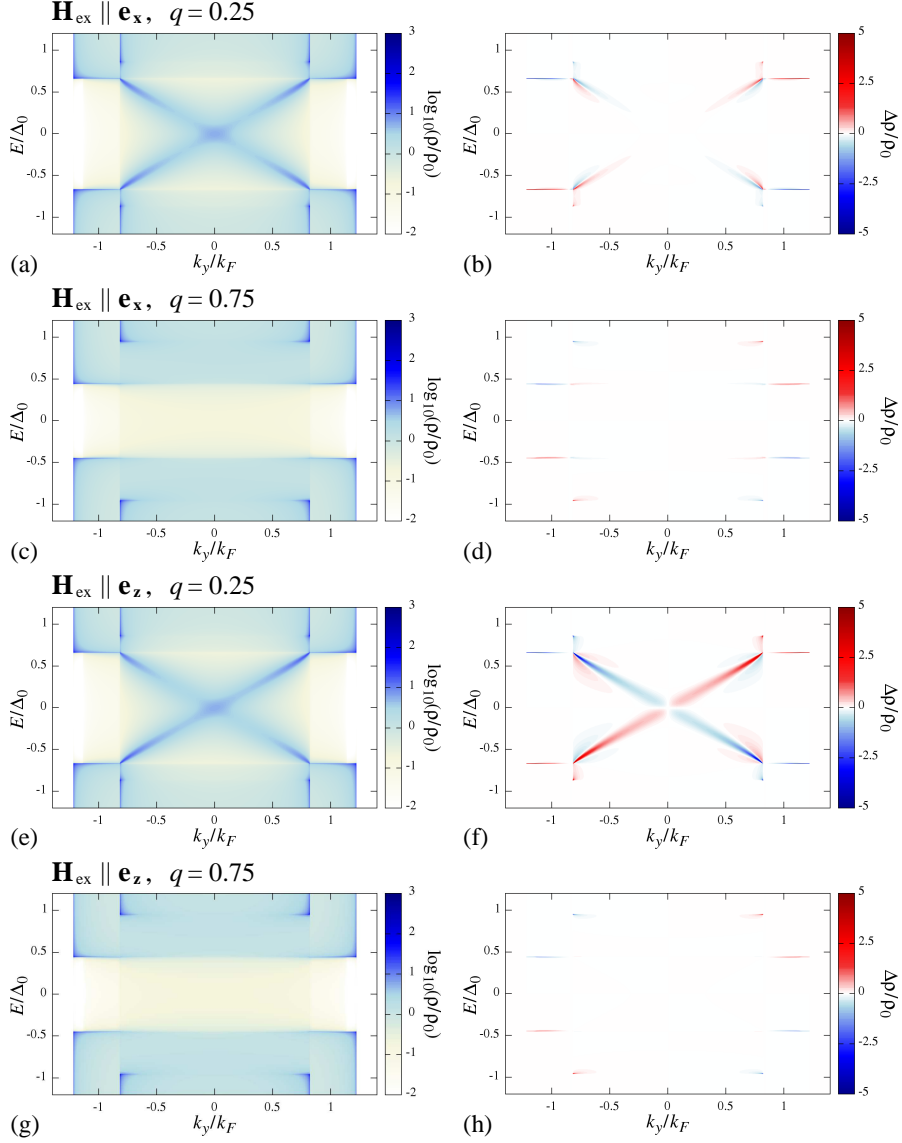
Figure 5. Zero-temperature energy- and momentum-resolved LDOS in the $(s+p)$-wave NCS at the interface with the FM. We present typical results for both x- and z-FM polarizations with $h_{\rm ex} = 0.3$, and also both the majority-triplet and majority-singlet pairing states. The left column shows the LDOS, while the right gives the momentum-antisymmetrized LDOS $\Delta\rho(E, k_y, x) = (\rho(E, k_y, x) - \rho(E, -k_y, x))/2$, both normalized by $\rho_0 = m/\pi\hbar^2 k_F \sqrt{1 + \tilde{\lambda}^2}$. We assume an intrinsic broadening of $5 \times 10^{-4}\Delta_0$.

wavefunction. It follows that for the helical superconductor the broadening of the two edge states is the same when the FM is polarized along the x- or y-axis, and there is hence vanishing interface current.

It is not possible to rigorously make the above argument in the presence of spin-orbit coupling or of a singlet gap. We nevertheless expect that the spin-dependent broadening of the edge states should be robust to these complications, as the spectrum evolves continuously as they are switched on. These spin-mixing terms may also lead to a similar broadening effect for an FM polarized along the x-axis, as they lift the degeneracy of the positive- and negative-helicity states [35]. To test this, we plot in figure 5 the energy- and momentum-resolved LDOS at the interface for systems representing both topologically nontrivial and trivial states and also both magnetization directions. An asymmetry in $\rho(E, k_y, x = 0^-)$ is readily visible only for the case of a majority-triplet pairing state and a z-polarized FM [panel (e)]: the right-moving subgap state is clearly less broadened than the left-moving state. Subtle changes in the LDOS are nevertheless present for the other cases, which can be revealed by plotting the momentum-antisymmetrized quantity

$$\Delta\rho(E, k_y, x = 0^-) = \frac{1}{2}\left[\rho(E, k_y, x = 0^-) - \rho(E, -k_y, x = 0^-)\right] \quad (21)$$

in the right column of figure 5. The different broadening of the two subgap states for the $q = 0.25$ NCS in contact with a z-polarized FM [panel (f)] now becomes much clearer. On the other hand, the results for the $q = 0.25$ NCS in contact with an x-polarized FM [panel (b)] reveal that the $k_y > 0$ and $k_y < 0$ states have been slightly shifted to higher and lower energies, respectively. This is consistent with the coupling of their spin polarization to the exchange field [37]; a similar but smaller energy shift for the z-polarized FM is masked in figure 5(f) by a much greater broadening. Closer inspection of the subgap states in figure 5(b) nevertheless reveals that the right-moving state is less broadened than the left-moving state, although the difference in linewidths is much smaller than for the z-polarized FM. For the majority-singlet cases, the antisymmetrized LDOS reveals that the changes in the LDOS are small and restricted to the gap edges.

This analysis shows that the unequal broadening of the right- and left-moving edge states is a plausible explanation for the enhanced current in the topologically nontrivial state, and also why there is a much larger current for the z-polarized FM. Furthermore, it explains why a sharp jump in the current across the topological transition was not anticipated by the exact-diagonalization calculations presented in Ref. [37]. The broadening of the edge states is dependent on an imperfect reflectivity, so that spectral weight can leak into the FM. Clearly this is only possible for a metallic FM; furthermore, in our ballistic-limit calculation we require that the FM be of width much larger than the NCS's coherence length, so that electron and hole pairs decohere before being reflected back at the opposite side of the FM towards the superconductor. In contrast, in Ref. [37] an insulating FM was considered, which obviously preserves the perfect edge reflectivity, and indeed no broadening of the edge states was found. The resulting edge current therefore has completely different characteristics to that found here, as it is due entirely to the induced x-spin polarization via the spin-orbit coupling.
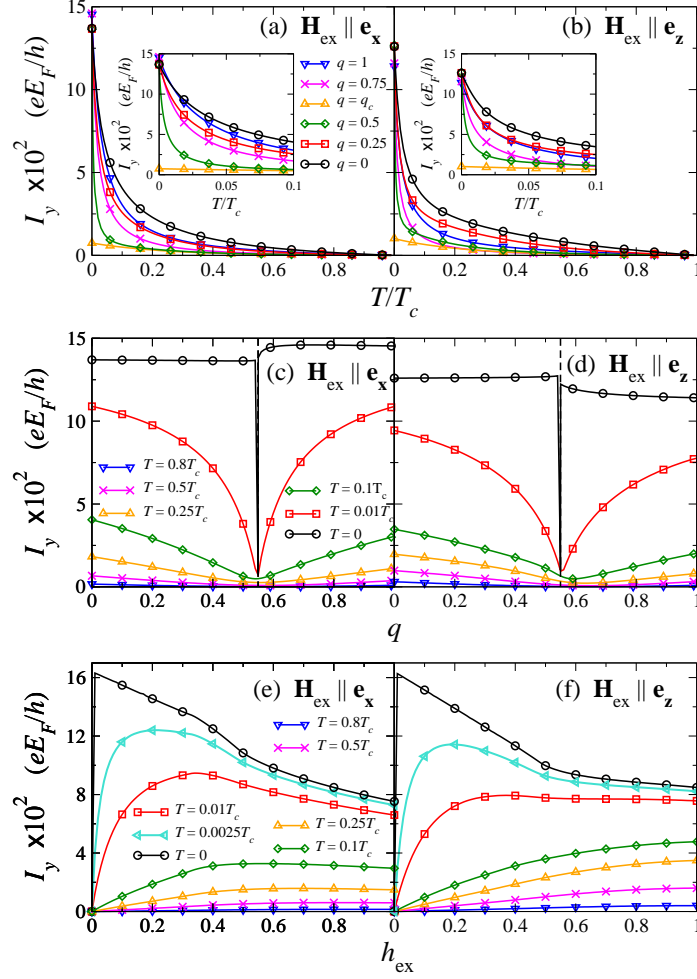
Figure 6.   Interface currents in the $(d_{xy}+p)$-wave NCS for a FM polarized along the x-axis (left column) and z-axis (right column). Current as a function of: (a), (b) temperature T for exchange-field strength $h_{ex} = 0.3$, with insets showing low-temperature $T \leq 0.1\,T_c$ currents in more detail; (c), (d) singlet-triplet parameter q for exchange-field strength $h_{ex} = 0.3$, where the vertical dashed line indicates the critical value q_c; (e), (f) exchange-field strength h_{ex} for singlet-triplet parameter $q = 0.25$.

3.2. $(d_{xy}+p)$-wave pairing state

As shown in figure 6, the currents in the $(d_{xy}+p)$-wave NCS are dramatically different from those in the $(s+p)$-wave state. We first note that the sign of the currents is reversed between the two cases, originating from the additional π phase shift acquired by Andreev-reflected quasiparticles due to the d_{xy} form factor. In further contrast to the $(s+p)$-wave case, the currents due to an x- and z-polarized FM are quantitatively very similar. More remarkable is the temperature-dependence of the current [panels (a) and (b)], which is characterized by a sharp increase at low temperatures for all $q \neq q_c$; for $q = q_c$, in contrast, the current grows only slightly below $T = 0.1\,T_c$, see

the insets of panels (a) and (b). As seen in panels (c) and (d), the magnitude of the zero-temperature current for $q \neq q_c$ far exceeds that in the $(s+p)$-wave case. The zero-temperature current is discontinuous at q_c: exactly at this point it takes a value roughly an order of magnitude smaller than at $q = q_c \pm 0^+$. There also appears to be a small jump in the current between q on either side of q_c, accompanied by a change of the slope. The difference between the current in the majority-triplet and majority-singlet regimes is nevertheless much smaller than for the $(s+p)$-wave NCS. At low nonzero temperatures, however, the current is sharply suppressed as one approaches $q = q_c$, indicating that the low temperature enhancement becomes increasingly sharp near the negative-helicity gap closing, e.g., see the $q = 0.5$ curve in the insets of panels (a) and (b). Indeed, the absence of the low-temperature current enhancement for $q = q_c$ implies that it crucially involves the negative-helicity states.

The dependence of the current on the exchange field [figures 6(e) and (f)] shows a remarkable deviation from linear-response behaviour at low temperatures: for $T \lesssim 0.01 \, T_c$ the current grows very rapidly with the exchange-field strength, before going through a maximum and slowly decreasing. At zero temperature an infinitesimally small exchange field in the FM is sufficient to generate a large current in the NCS. We note that there appears to be a qualitative change in the dependence of the zero-temperature current on the exchange field at $h_{\mathrm{ex}} \approx 0.5$, characterized by a change of slope of the low-temperature currents.

The momentum-resolved current (figure 7) shows that the low-temperature enhancement of the current is due entirely to states at $k_{F,+} < |k_y| < k_{F,-}$, consistent with the critical role of the negative-helicity gap deduced above. Although there is considerable variation of this current as a function of q for $T = 0.1 \, T_c$ [figures 7(a) and (b)], at zero temperature there is no variation with q for $q \neq q_c$ (not shown), for the same reasons as in the $(s+p)$-wave case. Thus, the change in the total zero-temperature current across the triplet-singlet boundary [figures 6(c) and (d)] is due only to states at $|k_y| < k_{F,+}$. The temperature-dependence of the $k_{F,+} < |k_y| < k_{F,-}$ current is astonishing: comparing the $T = 0.01 \, T_c$ and $T = 0$ curves in figures 7(c) and (d), we observe that while the current at $|k_y| < k_{F,\uparrow}$ has almost saturated to its zero-temperature value by $T = 0.01 \, T_c$, for $k_{F,\uparrow} < |k_y| < k_{F,-}$ the current more than doubles as the temperature is lowered. For $q = 0.25$, the the zero-temperature current at $k_{F,\uparrow} < |k_y| < k_{F,-}$ accounts for more than 40% of the total. Interestingly, in this momentum range the current displays a linear dependence upon k_y, and is almost independent of the exchange-field strength [figures 7(e) and (f)]. The current at $k_{F,\uparrow} < |k_y| < k_{F,-}$ is therefore clearly somewhat special, and its disappearance when $k_{F,\uparrow} = k_{F,-}$ at the exchange-field strength $h_{\mathrm{ex}} \approx 0.49$ closely matches the qualitative change in the exchange-field dependence seen in figures 6(e) and (f). In closing, we note that although the momentum-resolved currents at $|k_y| \gtrsim k_F$ are very similar for the two polarization orientations, clear differences are seen at smaller momenta.

The remarkable temperature dependence of the current in the $(d_{xy}+p)$-wave NCS is intimately connected to the coupling of the exchange field to the topological edge states at $k_{F,+} < |k_y| < k_{F,-}$. In Ref. [37] it was shown that at a vacuum edge these states possess strong x- and z-spin polarization, with equal magnitude but opposite sign at k_y and $-k_y$, as required by time-reversal symmetry. Applying an exchange field to the edge of the NCS therefore shifts these states in opposite directions, one above and the other below the Fermi energy. From (16) we see that the first term in the zero-temperature momentum-resolved current is proportional to the difference in the number of states below the Fermi energy at k_y and $-k_y$, while the second is
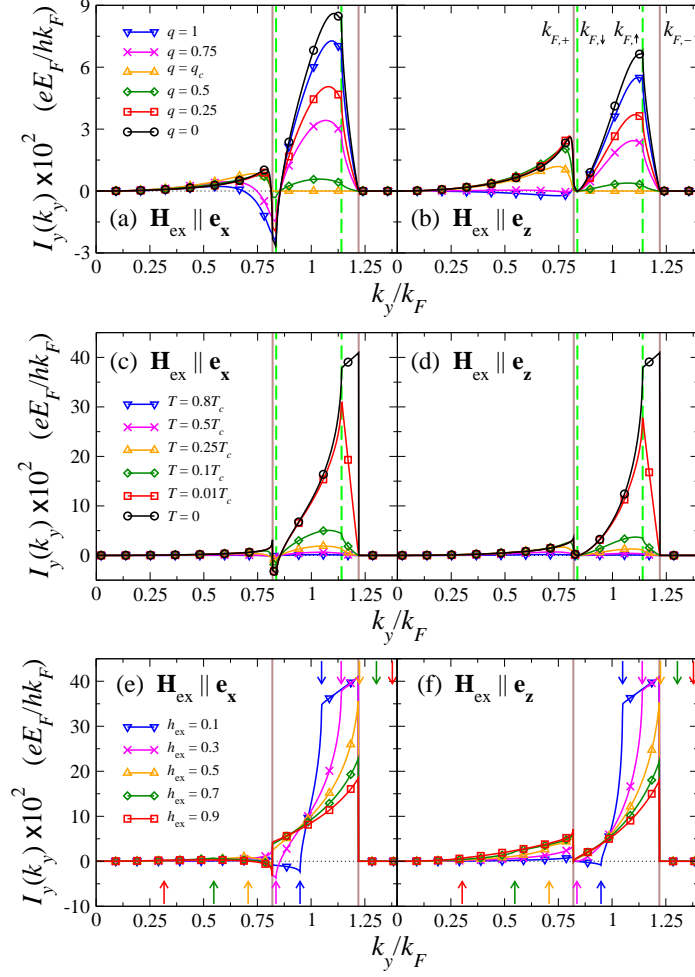
Figure 7. Momentum-resolved interface current in the $(d_{xy}+p)$-wave NCS for a FM polarized along the x-axis (left column) and z-axis (right column). We show the momentum-resolved current: (a), (b) for various values of the singlet-triplet parameter q at temperature $T = 0.1\,T_c$ and exchange field $h_{\mathrm{ex}} = 0.3$; (c), (d) for various temperatures T at singlet-triplet parameter $q = 0.25$ and exchange field $h_{\mathrm{ex}} = 0.3$; (e), (f) for various exchange fields h_{ex} at zero temperature and singlet-triplet parameter $q = 0.25$. In all panels the vertical brown solid lines are the projections of the positive- and negative-helicity Fermi surfaces of the NCS. In (a)-(d) the projected majority and minority Fermi surfaces of the FM are given by the vertical green dashed lines, while in (e) and (f) they are indicated by the colored arrows.
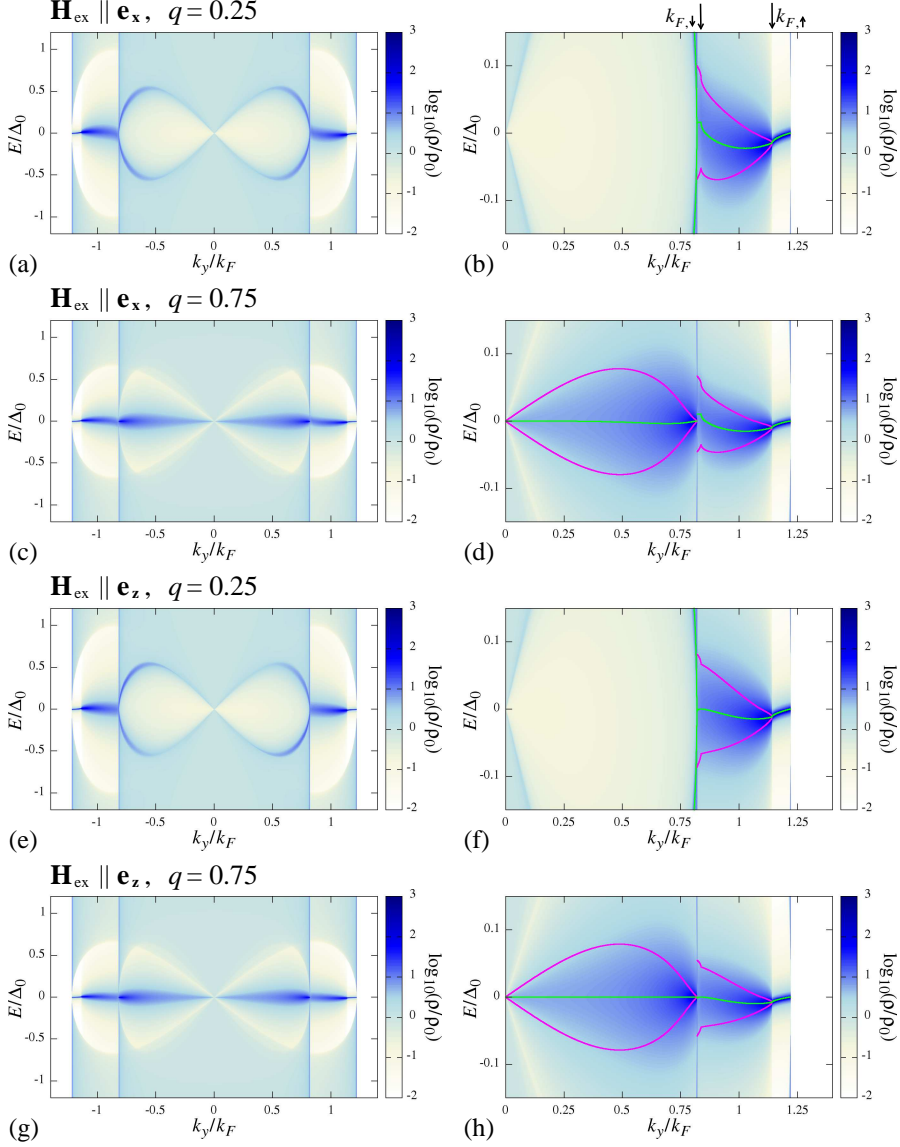
Figure 8. Zero-temperature energy- and momentum-resolved LDOS in the $(d_{xy}+p)$-wave NCS at the interface with the FM. We present typical results for both x- and z-FM polarizations with $h_{\mathrm{ex}} = 0.3$, and also both the majority-triplet and majority-singlet pairing states. The left column shows the LDOS for momenta $|k_y| < 1.4 k_F$ and energies $|E| < 1.2 \Delta_0$, while the right column shows a low-energy detail for $k_y > 0$. In the latter, the light green and dark magenta lines indicate the location of the peak in the subgap LDOS and its FWHM, respectively. In panel (b) we indicate the projection of the majority- and minority-spin Fermi surfaces in the FM. In all panels the LDOS is normalized by $\rho_0 = m/\pi\hbar^2 k_F \sqrt{1 + \tilde{\lambda}^2}$, and we assume an intrinsic broadening $5 \times 10^{-4} \Delta_0$.

proportional to the sum of the x-spin polarization at these momenta. The opposite energy shifts of the oppositely polarized flat-band states at k_y and $-k_y$ thus can contribute a large current. This implies the breakdown of linear-response behaviour at zero temperature, as then even an infinitesimal energy shift of these states causes a discrete change in the number difference and the x-spin polarization.

For the device studied here, this argument can be directly applied for $k_{F,\uparrow} < |k_y| < k_{F,-}$ where only evanescent solutions are possible in the FM and so the subgap states in the NCS have zero broadening. As seen in the LDOS plots in figure 8, these states acquire an energy shift $\lesssim 0.01\Delta_0$ from the coupling to the exchange field. From (16), we find that the zero-temperature momentum-resolved current for these states has the form

$$I_y(k_y) = \frac{eE_F}{4\pi\hbar k_F^2} \frac{k_{F,+}}{k_{F,-}} k_y \tag{22}$$

in the $h_{\mathrm{ex}} \to 0$ limit. The induced polarization at finite values of the exchange field can slightly reduce this current, as seen in figures 7(e) and (f). Although the momentum-resolved current (22) vanishes with the positive-helicity Fermi surface as the spin-orbit coupling strength diverges, the momentum-integrated zero-temperature current nevertheless saturates at $eE_F/4\pi\hbar$ in this limit. Much larger values of the low-temperature current than presented here are thus theoretically possible. Because of the small correction to the energy of the flat-band states, their contribution to the current only develops at extremely low temperatures $T < 0.01\,T_c$, which is indeed observed in figures 7(c) and (d). We note the apparent paradox that in spite of the strong spin-polarization of these states at $|k_y| = k_{F,-}$ [37], the LDOS plots show that the energy shift vanishes as $|k_y| \to k_{F,-}$, indicating that the states are "anchored" to the node of the negative-helicity gap. This is consistent with the observation that the current saturates at ever lower temperatures as one approaches $\pm k_{F,-}$ (not shown).

The flat-band states at $k_{F,+} < |k_y| < k_{F,\uparrow}$ also acquire an energy shift due to the coupling to the exchange field, but the presence of the open scattering channel in the ferromagnet also gives them a finite lifetime. This could not be anticipated by the analysis in Ref. [37], as discussed in section 3.1 above. In the right column of figure 8, we mark the maximum in the subgap LDOS by the green lines; the broadening is quantified by the full width at half maximum (FWHM) curves shown in magenta. The increasing broadening as $|k_y| \to k_{F,+}$ results in a rapid suppression of the zero-temperature momentum-resolved current, as the imbalance between the integrated weight at $-k_y$ and k_y is reduced. On the other hand, the broadening allows the current to saturate at temperatures well above the energy of the subgap maximum. Remarkably, it still seems possible to think of the current in terms of the energy shift of the subgap state, even when this is much smaller than the broadening. For example, the zero-crossing of the subgap maximum at $|k_y| \approx k_{F,\downarrow}$ for the x-polarized FM is nicely correlated with a sign change in the momentum-resolved current [see figures 7(a) and (e)], as expected from treating the subgap maximum as an unbroadened state. We note that there is no zero crossing of the subgap maximum for the z-polarized FM, and also no sign change in the current.

In closing, we note that the LDOS also shows significant structure for states lying within the projected positive-helicity Fermi surface ($|k_y| < k_{F,+}$), i.e., broadened dispersing states for majority-triplet pairing, and zero-energy states for majority-singlet pairing. Although in the latter case there is a slight shift in the location of the subgap maximum, the large broadening washes out any contribution to the current, except perhaps for $|k_y|$ very close to $k_{F,+}$.

4. Experimental prospects

The interface currents in the NCS-FM junction discussed above contain clear signatures of the topological state of the NCS. For the $(s+p)$-wave NCS this is the sharp jump in the current at the topological phase transition, while the presence of the topologically protected flat bands in the $(d_{xy}+p)$-wave NCS directly leads to the sharp increase of the current at low temperatures and a nonperturbative dependence on the exchange-field strength. The detection of any of these effects would therefore be strong evidence for a nontrivial topology of the NCS. The current characteristics of the $(d_{xy}+p)$-wave NCS are of particular interest as they only arise from nondegenerate flat bands. In contrast, previous proposals to evidence the flat bands by tunneling conductance measurements cannot easily distinguish between nondegenerate and doubly degenerate states [11, 30, 31, 32].

The experimental verification of our predictions is nevertheless likely to be challenging, and must overcome a number of obstacles. Foremost is the Meissner effect, as screening in the NCS will exactly compensate the interface current (19) for the half-space geometry considered here. For an NCS of finite width W, however, this problem can be avoided by exploiting the different length scales of the interface and screening current densities, the coherence length ξ_0 and the penetration depth λ_L, respectively. The best NCS topological superconductor candidates are extreme type-II superconductors, e.g., CePt$_3$Si has Ginzburg-Landau parameter $\kappa = \lambda_L/\xi_0 \approx 140$ [18]. For such a material it is possible to choose the sample width such that $\xi_0 \ll W \ll \lambda_L$, which implies that while our calculation for the edge currents remains valid, screening currents are very small. The penetration of the FM's magnetic field into the bulk NCS must then be considered: although the NCS pairing state is robust to weak fields along the z-axis, which are more easily kept outside of the NCS in any case, a field along the x-axis can destabilize the NCS towards a phase where the Cooper pairs acquire a finite momentum [39, 40]. Because the consequences of this for the edge states is unknown, a z-polarized FM is therefore a more favorable choice for experimental study.

The construction of an NCS-FM heterostructure device presents further difficulties. Firstly, some degree of surface roughness is unavoidable, which will lead to additional broadening of the interface states [50]. As long as this does not introduce further energy shifts, however, we expect that the interface current should persist for weak disorder. Indeed, we have seen above that even the strongly broadened edge states of the $(d_{xy}+p)$-wave NCS contribute a significant current. A more serious problem is the choice of material for the NCS part of the device. Although there are many examples of bulk NCS, little work has been done on incorporating them into heterostructures. An alternative approach is to instead engineer the NCS in the heterostructure, say by coating a superconducting substrate with a thin normal layer of a material with strong spin-orbit coupling, so that the former induces a superconducting gap in the latter. This is in the same spirit as the well-known proposal to artificially create a topological superconductor in a quantum wire [51, 52], which has been reported in recent experiments [53]. All suggestions along these lines [51, 52, 54, 55, 56, 57, 58] involve the modification of the standard proximity-induced superconductivity by spin-orbit coupling of the same form present in a bulk NCS. Using unconventional d-wave cuprate [57] or $s_{\pm}$-wave pnictide [58] superconductors holds particular promise, as it might then be possible to artificially create the most interesting cases of $(d_{xy}+p)$-wave or topologically nontrivial $(s+p)$-wave NCS, respectively. No matter how the NCS-FM heterostructure is constructed,

however, there will be some variation of the superconducting gaps close to the interface due to the pair-breaking effect of the tunneling barrier and the FM [59]. Although our calculation does not account for this, the current predicted above should be robust as it ultimately arises from the spin structure of the bulk condensate.

5. Summary

In this paper we have used a quasiclassical method to study the properties of the charge current that appears at the interface between an NCS and a metallic FM in a two-dimensional junction, where each phase is assumed to occupy a half space. We have considered two complementary models of the NCS: a gapped $(s+p)$-wave pairing state, and a gapless $(d_{xy}+p)$-wave system. Due to the contrasting topological structure of the two models, we find completely different dependences of the interface current on the temperature, the exchange-field strength h_{ex} and the singlet-triplet parameter q. In both cases we find signatures of the topology in the interface transport. For the $(s+p)$-wave NCS, the topological transition from the nontrivial to the trivial state is signaled by a discontinuous drop in the zero-temperature current, due to the disappearance of the contribution from the subgap states. In the $(d_{xy}+p)$-wave NCS, there is an enormous enhancement of the current as the temperature approaches zero, and the dependence on the exchange-field strength becomes singular. This anomalous behaviour originates from the energy shifts of the spin-polarized flat bands due to the coupling to the exchange field in the FM. While the results for the $(d_{xy}+p)$-wave NCS were anticipated by the analysis of an exchange field applied directly to the edge [37], the current in the $(s+p)$-wave NCS is qualitatively different due to the broadening of the subgap states by tunneling into the metallic FM. We thus find that the mechanism based on flat bands, relevant for the $(d_{xy}+p)$-wave case, is rather robust and independent of the detailed nature of the FM. Hence, one can speculate that similar current characteristics might also be realized in other systems possessing topologically protected nondegenerate flat bands.

Acknowledgments

References

[1] Schnyder A P, Ryu S, Furusaki A and Ludwig A W W 2008 *Phys. Rev. B* **78** 195125
[2] Kitaev A Y 2009 *AIP Conf. Proc.* **1134** 22
[3] Hasan M and Kane C 2010 *Rev. Mod. Phys.* **82** 3045
[4] Ryu S, Schnyder A P, Furusaki A and Ludwig A W W 2010 *New J. Phys.* **12** 065010
[5] Qi X-L and Zhang S-C 2011 *Rev. Mod. Phys.* **83** 1057
[6] Sato M 2006 *Phys. Rev. B* **73** 214502
[7] Béri B 2010 *Phys. Rev. B* **81** 134515
[8] Volovik G E 2011 *JETP Lett.* **93** 66
    Heikkilä T T, Kopnin N B and Volovik G E 2011 *JETP Lett.* **94** 233
[9] Yada K, Sato M, Tanaka Y and Yokoyama T 2011 *Phys. Rev. B* **83** 064505
[10] Schnyder A P and Ryu S 2011 *Phys. Rev. B* **84** 060504(R)
[11] Schnyder A P, Brydon P M R and Timm C 2012 *Phys. Rev. B* **85** 024522
[12] Dahlhaus J P, Gibertini M and Beenakker C W J 2012 *Phys. Rev. B* **86** 174520

[13] Matsuura S, Chang P-Y, Schnyder A P and Ryu S 2012 arXiv:1212.2673
[14] Wan X, Turner A M, Vishwanath A and Savrasov S Y 2011 *Phys. Rev. B* **83** 205101
[15] Turner A M and Vishwanath A 2013 arXiv:1301.0330
[16] Zhao Y X and Wang Z D 2012 arXiv:1211.7241
[17] Frigeri P A, Agterberg D F, Koga A and Sigrist M 2004 *Phys. Rev. Lett.* **92** 097001
[18] Bauer E and Sigrist M (eds) 2012 *Non-Centrosymmetric Superconductors: Introduction and Overview* (*Lecture Notes in Physics* vol 847) (Berlin: Springer)
[19] Bauer E, Hilscher G, Michor H, Paul C, Scheidt E W, Gribanov A, Seropegin Y, Noël H, Sigrist M and Rogl P 2004 *Phys. Rev. Lett.* **92** 027003
[20] Kimura N, Ito K, Saitoh K, Umeda Y, Aoki H and Terashima T 2005 *Phys. Rev. Lett.* **95** 247004
[21] Sugitani I *et al.* 2006 *J. Phys. Soc. Jpn.* **75** 043703
[22] Yuan H Q, Agterberg D F, Hayashi N, Badica P, Vandervelde D, Togano K, Sigrist M and Salamon M B 2006 *Phys. Rev. Lett.* **97** 017006
        Nishiyama N, Inada Y and Zhen G-q 2007 *Phys. Rev. Lett.* **98** 047002
[23] Chen J, Salamon M B, Akutagawa S, Akimitsu J, Zhang J L, Jiao L and Yuan H Q 2011 *Phys. Rev. B* **83** 144529
[24] Mondal M, Joshi B, Kumar S, Kamlapure A, Ganguli S C, Thamizhavel A, Mandal S S, Ramakrishnan S and Raychaudhuri P 2012 *Phys. Rev. B* **86** 094520
[25] Qi X-L, Hughes T L, Raghu S and Zhang S-C 2009 *Phys. Rev. Lett.* **102** 187001
[26] Sato M and Fujimoto S 2009 *Phys. Rev. B* **79** 094504
[27] Qi X-L, Hughes T L and Zhang S-C 2010 *Phys. Rev. B* **81** 134508
[28] Yip S-K 2010 *J. Low Temp. Phys.* **160** 12
[29] Tanaka Y, Yokoyama T, Balatsky A V and Nagaosa N 2009 *Phys. Rev. B* **79** 060505(R)
[30] Tanaka Y, Mizuno Y, Yokoyama T, Yada K and Sato M 2010 *Phys. Rev. Lett.* **105** 097002
[31] Sato M, Tanaka Y, Yada K and Yokoyama T 2011 *Phys. Rev. B* **83** 224511
[32] Brydon P M R, Schnyder A P and Timm C 2011 *Phys. Rev. B* **84** 020501(R)
[33] Iniotakis C, Hayashi N, Sawa Y, Yokoyama T, May U, Tanaka Y and Sigrist M 2007 *Phys. Rev. B* **76** 012501
[34] Vorontsov A B, Vekhter I and Eschrig M 2008 *Phys. Rev. Lett.* **101** 127003
[35] Lu C-K and Yip S-K 2010 *Phys. Rev. B* **82** 104501
[36] Yokoyama T, Onari S and Tanaka Y 2007 *Phys. Rev. B* **75** 172511
[37] Schnyder A P, Timm C and Brydon P M R 2013 arXiv:1302.3461
[38] Wong C L M, Liu J, Law K T and Lee P A 2012 arXiv:1206.5601
[39] Agterberg D F and Kaur R P 2007 *Phys. Rev. B* **75** 064511
[40] Loder F, Kampf A P and Kopp T 2012 arXiv:1206.1816
[41] Duckheim M and Brouwer P W 2011 *Phys. Rev. B* **83** 054513
[42] Annunziata G, Cuoco M, Noce C, Sudbø A and Linder J 2011 *Phys. Rev. B* **83** 060508(R)
        Annunziata G, Manske D and Linder J 2012 *Phys. Rev. B* **86** 174514
[43] Molenkamp L W, Schmidt G and Bauer G E W 2001 *Phys. Rev. B* **64** 121202(R)
        Zülicke U and Schroll C 2001 *Phys. Rev. Lett.* **88** 029701
        Matsuyama T, Hu C-M, Grundler D, Meier G and Merkt U 2002 *Phys. Rev. B* **65** 155322
[44] McMillan W L 1968 *Phys. Rev.* **175** 559
[45] Ishii C 1970 *Prog. Theor. Phys.* **44** 1525
[46] Furusaki A and Tsukada M 1991 *Solid State Commun.* **78** 299
[47] Kashiwaya S and Tanaka Y 2000 *Rep. Prog. Phys.* **63** 1641
[48] Furusaki A, Matsumoto M and Sigrist M 2001 *Phys. Rev. B* **64** 054514
[49] Stone M and Roy R 2004 *Phys. Rev. B* **69** 184511
[50] Matsumoto M and Shiba H 1995 *J. Phys. Soc. Jpn.* **64** 1703
[51] Sau J D, Lutchyn R M, Tewari S and Das Sarma S 2010 *Phys. Rev. Lett.* **104** 040502
        Lutchyn R M, Sau J D and Das Sarma S 2010 *Phys. Rev. Lett.* **105** 077001
[52] Oreg Y, Refael G and von Oppen F 2010 *Phys. Rev. Lett.* **105** 177002
[53] Mourik V, Zuo K, Frolov S M, Plissard S R, Bakkers E P A and Kouwenhoven L P 2012 *Science* **336** 1003
[54] Fu L and Kane C L 2008 *Phys. Rev. Lett.* **100** 096407
[55] Chung S B, Zhang H-J, Qi X-L and Zhang S-C 2011 *Phys. Rev. B* **84** 060510
[56] Potter A C and Lee P A 2012 *Phys. Rev. B* **85** 094516
[57] Takei S, Fregoso B M, Galitski V and Das Sarma S 2013 *Phys. Rev. B* **87** 014504
[58] Zhang F, Kane C L and Mele E J 2012 arXiv:1212.4232
[59] Buzdin A I 2005 *Rev. Mod. Phys.* **77** 935
        Begeret F S, Volkov A F and Efetov K B 2005 *Rev. Mod. Phys.* **77** 1321